Catalytic Locomotion of Core-Shell Nanowire Motors

Bumjin Jang,[†] *Wei Wang,*[‡,¶] *Samuel Wiget,*[†] *Andrew J. Petruska,*[†] *Xiangzhong Chen,*[†] *Chengzhi Hu,*[†] *Ayoung Hong,*[†] *David Folio,*[§] *Antoine Ferreira,*[§] *Salvador Pané,**[,†] *and Bradley J. Nelson**[,†]

[†]Institute of Robotics and Intelligent Systems, ETH Zurich, Zurich, CH-8092, Switzerland

[‡]Shenzhen Key Laboratory for Advanced Materials, School of Material Sciences and Engineering, Shenzhen Graduate School, Harbin Institute of Technology, University Town, Shenzhen 518055, China

¶ Center for Soft and Living Matter, Institute for Basic Science (IBS), Ulsan 44919, Republic of Korea

[§] INSA Centre Val de Loire, Universite d'Orléans, PRISME EA 4229, Bourges, France.

Table of contents

S1. Numerical modeling procedures

Governing equations for electroosmotic locomotion. In general, the electroosmotic locomotion mechanism of a catalytic nanomotor can be expressed by coupling three governing equations as follows.[1, 2] First, the transport of protons by surface-redox reaction can be defined by the stationary convection-diffusion equation with electromigration. From the continuity equation this can be written as:

$$\nabla \cdot J_i = 0 = u \cdot \nabla c_i - D_i \nabla^2 c_i - \frac{z_i F D_i \nabla \cdot (c_i \nabla \phi)}{\mathrm{RT}} \quad \text{(S1)}$$

where J is the flux, u is the fluid velocity, c is the concentration, z is the charge, D is the diffusion constant, R is the gas constant, T is the temperature, and ϕ is electrostatic potential and F, the Faraday constant, and the subscript i denotes the species; in our case, i is H^+ and its counter ion (HCO_3^-).

Equation (S1) indicates that protons are transferred *via* diffusion, convection, and electromigration according to the right side of S1. The electrostatic potential (ϕ) can be coupled with the Poisson equation to obtain:

$$-\varepsilon \nabla^2 \phi = \rho_e = F(z_+ c_+ + z_- c_-) \quad \text{(S2)}$$

where ε is the permittivity of water, ρ_e is the space charge density, z_+ is the charge of H^+, and z_- is the charge of HCO_3^-. Equation (S2) indicates that the spatial distribution of an electric potential is developed by spatially distributed charges. The generated electric field causes an electroomotic flow around a negative-potential surface formed by the zeta potential of the nanomotor. The electroosmotic flow is determined by the stationary incompressible Navier-Stokes equations for a Newtonian fluid,

$$\nabla \cdot u = 0 \quad \text{(S3)}$$

$$\rho(u \cdot \nabla u) = -\nabla p + \eta \nabla^2 u - \rho_e \nabla \phi \quad \text{(S4)}$$

where, ρ is the density of water, p is the pressure, η is the dynamic viscosity of water, and $\rho_e \nabla \phi$ is the electroomosis force.

Defining parameters in COMSOL model. The three governing equations were coupled through the models of diluted species transport, electrostatics, and creeping flow, respectively, in COMSOL. Details in geometry, boundary conditions and meshes, were modified from a report as follows.[3]

A 2D axisymmetric approach was selected to save computing time. The geometry of our core-shell nanowire was defined as a simple rod (see, Figure S3. The rod had a diameter of 300 nm, but the length was varied (0.5, 1.5, 2.5 and 3.5 um) depending on our studies. A finite radius (20 nm) of curvature was introduced at the edges of the rod to avoid a geometrically singular result. This rod was further positioned in a water domain with a size of 50 um × 50 um.

The above-mentioned convection-diffusion, Poisson, and incompressible Navier-Stokes (for a Newtonian fluid) equations were coupled through the COMSOL models of diluted species transport, electrostatics, and creeping flow. The convection and electromigration terms were implemented to fulfill (S1). Inward and outward proton fluxes were defined on the surface of the rod to represent the oxidation and reduction reaction, respectively (see, Figure S3). According to the configuration of our Au/Ru core-shell nanowire, the outward flux of proton was assigned to a tip of the rod (Au anode) and sides (Ru cathode) were assigned to the inward proton flux. We used a proton outward flux of 7e-6 mol m^{-2} s^{-1}, the flux at 6 wt % H_2O_2. According to the charge conservation law of the continuity equation (S1), a proton outward flux was set as the inward flux multiplied by the anode/cathode surface area ratio. In addition, the bulk proton concentration was set to be 2.24e-3 mol m^{-3}, the value for saturated water with ambient CO_2 at pH 5.65.

In the electrostatic model, a space charge density was assigned to the water domain in order to solve the electrostatic potential according to the Poisson equation (S2). An electric potential of 0 V was used for all boundaries of the water domain.

Creeping flow boundaries were set as follows. The incompressible flow model was chosen in the physical model option. An open boundary condition with no viscous stress was set for the boundaries of the water domain. The electroosmotic boundary was set on the boundaries of the rod with a tangential electric field as the zeta potential of the core-shell nanowire and a relative permittivity of the water domain. In our case the measured zeta potential was approximately - 26 mV.

The meshes in the COMSOL model were defined as follows. While the element size of the mesh of the water domain was predefined as extra-fine, those of the rod were set to be 1e-6 um and 5e-7 um for maximum and minimum element size, respectively. The free triangular shape was used for the entire mesh.

Simulated speed as a function of the length of core-shell nanowire. The fluid flow around the nanowire's body was used to deduce the speed of core-shell nanowire using the previously reported equation,[3, 4]

$$U_{nanomotor} = -\frac{<\alpha U_{fluid}>}{<\alpha>} \quad \text{(S5)}$$

where $\alpha = \frac{1-2\ln(2\varepsilon(1-s^2)^{1/2})}{8(1-\ln\varepsilon)^2}$, and $\varepsilon = \frac{b_0}{L/2}$ (S6)

$U_{nanomotor}$ is the speed of nanomotor, U_{fluid} is the fluid velocity along the surface of the nanomotor, b_0 is the radius of the nanomotor, and L is the length of nanomotor. The position of L is *s* , scaled from -1 to 1.

S2. Numerical modelling results of the effect of core protrusion on the speed of nanomotors

One may consider that the experimentally observed speed difference among the material combination may originate from the core protrusion where a small segment of the core metal that is exposed as shown in Figure S4a. We acknowledge the possibility of having such a protruding feature during the releasing process of nanowires from the substrate *via* sonication. However, we note that the observed protrusions are mostly at nanoscale (less than 300 nm as seen in Figure S4a).

To further address the concern on how this protruding feature affects the motor's behavior, we conducted numerical simulation because it is easy to assess the localized fluid flow at nanoscale for nano-sized protrusions. Direct observations with optical microscopy are impossible due to limited optical resolution. For core-shell nanowires of a total length of 2.5 μm, two extreme cases of core protrusion were considered in the models as depicted in Figure S4b: case 1) a large protrusion of L_{core} = 0.3 μm (or L_{shell} = 2.2 μm) and case 2) a small protrusion (ideal case) of L_{core} = 0 μm (or L_{shell} = 2.5 μm). The simulation results of both cases show a decrease in maximum electropotential (Figure S5a and b) and fluid velocity (Figure S5c and d) near the core protrusion when decreasing L_{core}. This is because, as the cathode area (shell) increases, there is a decrease in the number of protons generated at the anode (protruded core), which in turn results in a decreased electroosmotic force. Figure S5e and f shows fluid profiles on the surface along the nanowire long axis. As expected, an overall decrease in fluid velocity was observed for the shorter L_{core}.

The fluid profile was further converted into motor speed by using Solomentsev and Anderson model, and yielded a motor speed of 4.70 μm/s and 1.45 μm/s for case (1) and (2), respectively (Figure S6a). With this modelling result, one may expect a variation in speeds of at most a few fold among motors of different compositions based on differences in degree of

protrusion. However, the experimentally observed speed of Au/Ru (~41 μm/s) core-shell nanowires is significantly larger than that of Au/Rh (~3.2 μm/s) (Figure S6b). This noticeable speed difference between the numerical modelling and experiment serves as the motivation for us to explore an alternative mechanism on the motion of our core-shell nanowires.

References

(1) Moran, J. L.; Wheat, P. M.; Posner, J. D. Locomotion of Electrocatalytic Nanomotors Due to Reaction Induced Charge Autoelectrophoresis. *Phys. Rev. Lett. E* **2010**, *81*, 065302.

(2) Moran, J. L.; Posner, J. D. Electrokinetic Locomotion Due to Reaction-Induced Charge Auto-Electrophoresis. *J. Fluid Mech.* **2011**, *680*, 31-66.

(3) Wang, W.; Chiang, T. Y.; Velegol, D.; Mallouk, T. E. Understanding the Efficiency of Autonomous Nano- and Microscale Motors. *J. Am. Chem. Soc.* **2013**, *135*, 10557-10565.

(4) Solomentsev, Y.; Anderson, J. L. Electrophoresis of Slender Particles. *J. Fluid Mech.* **1994**, *279*, 197-215.

S3. Supporting figures

Figure S1. Schematic drawings of three different nanowires: (a) the conventional bimetallic nanowire,(b) the ideal core-shell nanowire, and (c) the core-shell nanowire, studied in this paper.

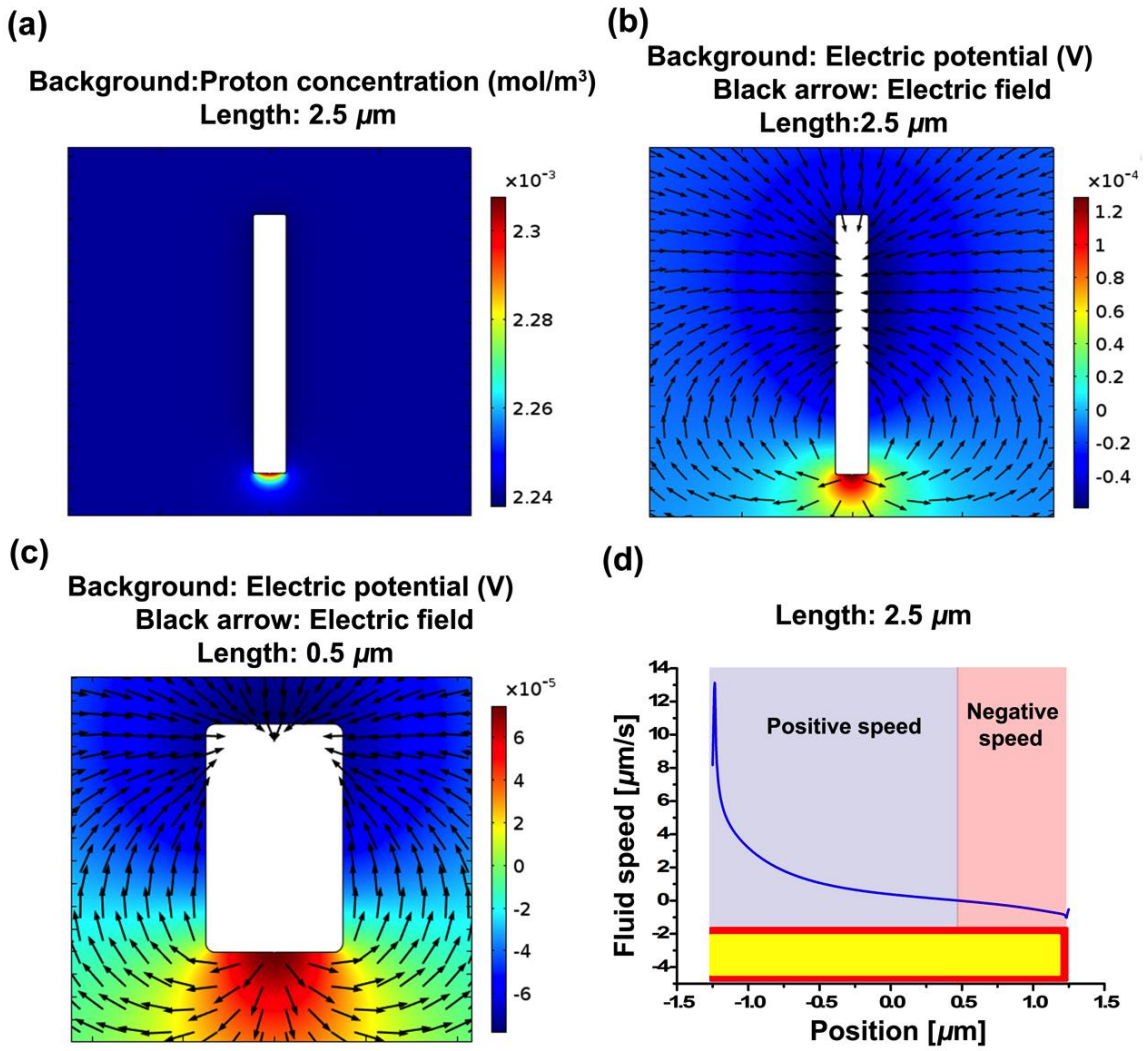

Figure S2. Numerical modeling of Au/Ru core-shell nanowires in the presence of H_2O_2: (a) Proton concentration (background) for a length of 2.5 um. (b), (c) Electric potentials (background) and field (black arrows) for a length of 2.5 um and 0.5 um, respectively. (d) Fluid speed along to the nanowire (length of 2.5 um) long axis; the insert is a schematic drawing for the core-shell nanowire.

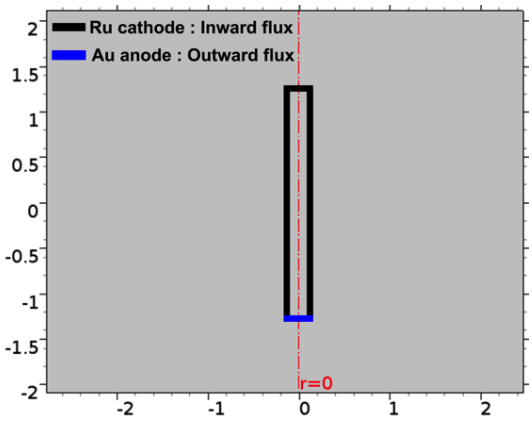

Figure S3. A defined geometry and proton fluxes for the simulation of a Au/Ru core-shell nanowire.

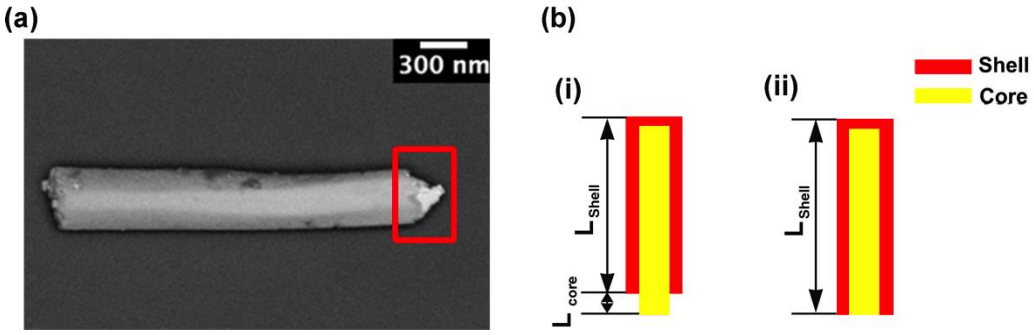

Figure S4. (a) The representative SEM image of the core protrusion: The image was obtained from a back scattering electron detector. The blight color in the inserted red box is assigned to be the protruded core. (b) The schematic drawings of the protruded cores of two different lengths: The lengths of the core protrusion are (i) 0.3 μm, and (ii) 0 μm. L_{shell} and L_{core} is the length of the shell and core protrusion, respectively. The total length is 2.5 μm.

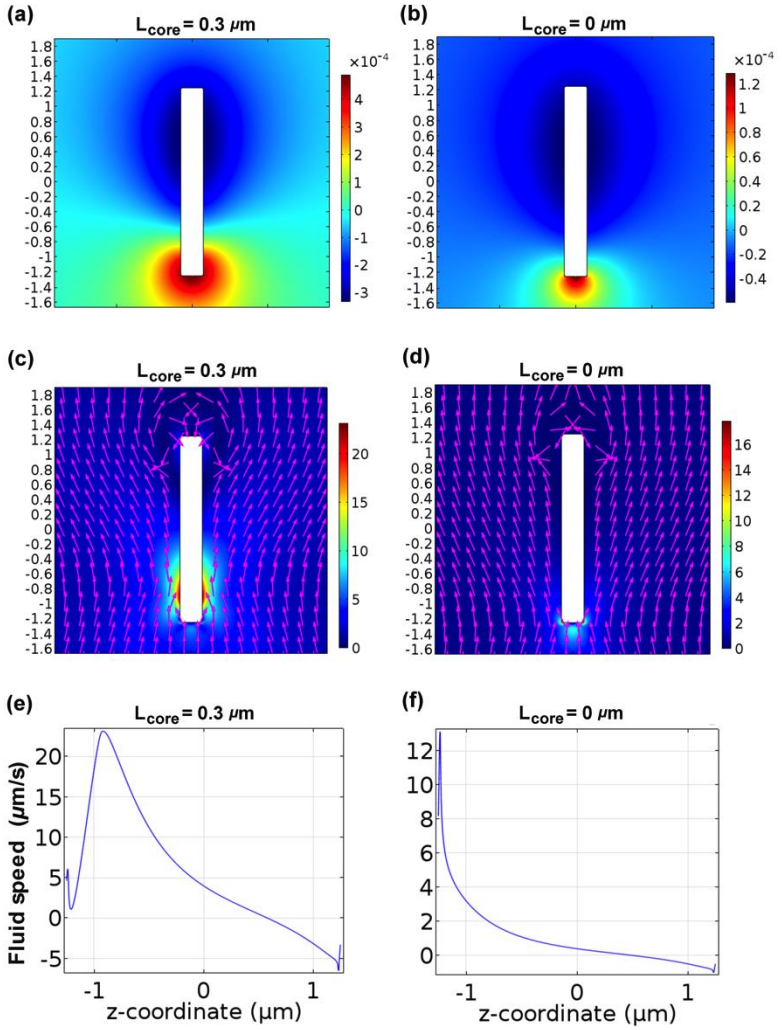

Figure S5. The numerical modelling of the core-shell nanowires with different lengths of the core protrusion: L_{core} = 0.3 μm, and 0 μm. (a) and (b): the simulated electropotential (background), (c) and (d): the simulated magnitude of fluid velocity (background), fluid flow (magenta arrows), and (e) and (f): the fluid profiles along the long axis of the core-shell nanowire. The fluid profiles on the left and the right side nanowire surfaces are identical.

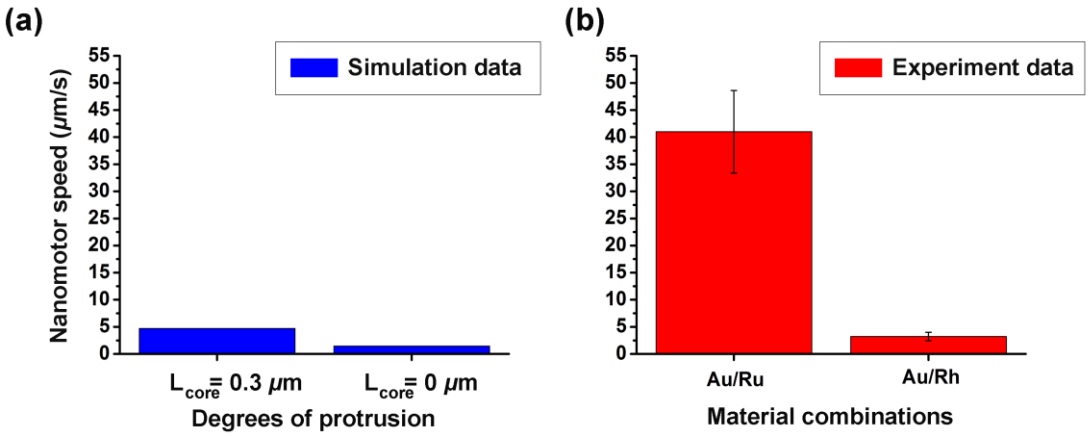

Figure S6. The speed of nanomotors: (a) Simulation results of the motor speed as a function of degrees of a protrusion, and (b) Experimental results of the speeds of Au/Ru and Au/Rh motors. The averaged speeds were obtained from at least 18 samples. 20 wt % of H_2O_2 solution was used for the experiment. It is clear that the relatively small variation as a result of protrusion cannot effectively account for the large variation in speeds between Au/Rh and Au/Ru core-shell nanomotors.

S4. Supporting movies

Movie S1. A motion comparison of Au/Ru core-shell nanowires at different lengths.

Movie S2. A motion comparison among Au/Rh, Rh/Au and Au/Ru core-shell nanowires.